Solar Phys
DOI 10.1007/s11207-009-9442-6

The Formation of Large-Scale Current Sheets within Magnetic Clouds

M.J. Owens

Received: 16 June 2009 / Accepted: 14 August 2009

Abstract Magnetic clouds are a class of interplanetary coronal mass ejections (CME) predominantly characterised by a smooth rotation in the magnetic field direction, indicative of a magnetic flux rope structure. Many magnetic clouds, however, also contain sharp discontinuities within the smoothly varying magnetic field, suggestive of narrow current sheets. In this study we present observations and modelling of magnetic clouds with strong current sheet signatures close to the centre of the apparent flux rope structure. Using an analytical magnetic flux rope model, we demonstrate how such current sheets can form as a result of a cloud's kinematic propagation from the Sun to the Earth, without any external forces or influences. This model is shown to match observations of four particular magnetic clouds remarkably well. The model predicts that current sheet intensity increases for increasing CME angular extent and decreasing CME radial expansion speed. Assuming such current sheets facilitate magnetic reconnection, the process of current sheet formation could ultimately lead a single flux rope becoming fragmented into multiple flux ropes. This change in topology has consequences for magnetic clouds as barriers to energetic particle propagation.

Keywords Coronal mass ejection · Energetic particle propagation · Magnetic cloud · Magnetic flux rope · Magnetic reconnection · Solar activity · Solar wind

1. Introduction

Magnetic clouds (MCs) are a subset of interplanetary coronal mass ejections (ICMEs) characterised primarily by a large-scale, smooth rotation in the magnetic field direction (Burlaga *et al.*, 1981). This signature is interpreted and modelled as a magnetic flux rope (Burlaga, 1988; Lepping, Jones, and Burlaga, 1990). On the small scale, however, the magnetic field is often found to be far from smooth, often exhibiting filamentary structure (Crooker *et al.*, 1990) which may be associated with *in situ* magnetic reconnection (Collier *et al.*, 2001;

M.J. Owens (✉)
Space and Atmospheric Physics, The Blackett Laboratory, Imperial College London, Prince Consort Road, London SW7 2BW, UK
e-mail: m.owens@imperial.ac.uk

Published online: 02 October 2009

Gosling *et al.*, 2007). Even on the large scale, the field often contains discontinuities, which is attributed to various external processes ranging from multiple interacting flux ropes (Osherovich, Fainberg, and Stone, 1999; Hu *et al.*, 2004; Steed *et al.*, 2008) and shocks travelling through magnetic clouds (Rees and Forsyth, 2004), to twisted fields resulting from cometary dust tails (Russell, Jian, and Luhmann, 2009).

In this study, it is demonstrated how large-scale current sheets can form within MCs solely from their kinematic propagation from the Sun to the Earth. In Section 2 we show an example of a classic magnetic cloud observed by the ACE spacecraft that displays a large discontinuity in the otherwise smooth magnetic field rotation. In Section 4, four such events are shown to be well-described by a kinematically distorted flux rope model. In Section 5 this model is used to investigate the current system associated with such a magnetic configuration.

2. Observations

Figure 1 shows a magnetic cloud encountered by the ACE spacecraft in March 2001. Data are shown at 1-h resolution to highlight the large-scale features (the left panels of Figure 3 shows the same magnetic field data at 5-min resolution). The event displays a smooth rotation in the magnetic field direction, indicative of a magnetic flux rope. A slowly declining velocity profile suggests the flux rope is still expanding as it passes over the observing spacecraft. Expansion in the radial direction is supported by the observed reduction in proton density and temperature relative to the ambient solar wind. Of particular interest to this study is the sharp discontinuity in the magnetic field direction approximately halfway through the magnetic field rotation, indicated by the blue dashed line. In this case, the discontinuity is concurrent with the magnetic field intensity maximum. Figures 3 and 4, discussed further in Section 4, show a further three examples of magnetic clouds with large magnetic field discontinuities close to the centre of the flux rope signature.

3. Magnetic Flux Rope Model

In coronagraph observations, CMEs frequently exhibit circular structures attributed to circular cross-section magnetic flux ropes (Low, 1994; Rust, 1994; Dere *et al.*, 1999; Savani *et al.*, 2009). Propagation with the radially expanding solar wind, however, causes a CME to maintain approximately constant angular width with respect to the Sun (*e.g.*, St. Cyr *et al.*, 2000; Schwenn *et al.*, 2005), and consequently become highly elongated in the non-radial direction (Newkirk, Hundhausen, and Pizzo, 1981; McComas *et al.*, 1988; Riley and Crooker, 2004). This kinematic distortion is incorporated into analytical models of ICME flux ropes (Owens, Merkin, and Riley, 2006), including the effect of a structured solar wind (Owens, 2006). Owens (2008) combined remote and *in situ* observations of a magnetic cloud to demonstrate that this cross-sectional elongation of a magnetic flux rope cannot be constrained on the basis of *in situ* observations alone. In this study, we adopt the same analytical model as Owens, Merkin, and Riley (2006), outlined briefly below. See Owens, Merkin, and Riley (2006) and Owens (2006) for a more detailed description of the model.

The model uses heliocentric cylindrical polar coordinates ($\hat{\mathbf{R}}$, $\hat{\theta}$, $\hat{\mathbf{Z}}$), with $\hat{\mathbf{Z}}$ aligned with the axis of the flux rope. Thus a two-dimensional geometry is considered throughout, and effects of axial-curvature of the flux rope are assumed to be negligible. At time $t = 0$, the

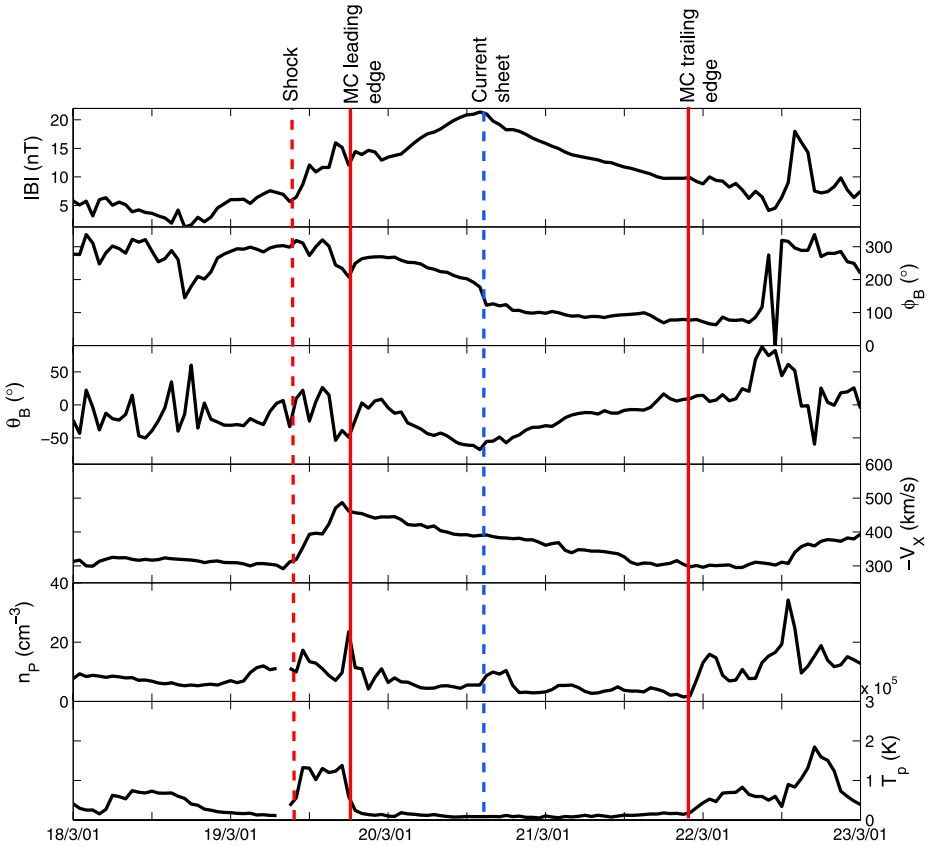

Figure 1 A magnetic cloud observed by the ACE spacecraft during March 2001. The panels, from top to bottom, show the magnetic field intensity, the GSE in-ecliptic and out-of-ecliptic angles of the magnetic field vector, the solar wind speed, proton density, and proton temperature. The shock location is shown by the vertical red dashed line, whereas the boundaries of the magnetic cloud are shown by the solid red vertical lines. The dashed blue line shows the location of a sharp discontinuity in the magnetic field direction.

magnetic cloud is assumed to take the form of a constant-α, force-free flux rope of radius r_0, axial field strength B_0, and helicity H at a position $P_R = h_0$, $P_\theta = 0$. The flux rope outer boundary is taken to be the distance from the axis at which the field becomes completely poloidal. Thus α (defined by $\mathbf{J} = \alpha\mathbf{B}$, $\mathbf{J}$ and $\mathbf{B}$ being the current density and magnetic field vectors, respectively) has a constant value of 2.408.

Positions within the flux rope are described by flux rope axis-centred polar coordinates $(\hat{\mathbf{r}}_{FR}, \hat{\phi})$, with $\phi = 0$ at $\theta = 0$. Each point within the flux rope moves subject to two velocities: expansion about the axis at speed $V_{EX} r_{FR}/r_0$ in the $\hat{\mathbf{r}}_{FR}$ direction and transit with the ambient solar wind in the $\hat{\mathbf{R}}$ direction at speed V_{TR}. To maintain a constant angular extent, as is frequently reported in coronagraph observations of CMES (*e.g.*, Hundhausen, 1993; St. Cyr *et al.*, 2000; Gopalswamy, 2004), it is necessary to limit the expansion velocity to the $\hat{\mathbf{R}}$ component. Thus at a time t, a point initially inside the flux rope at $\mathbf{P}_0 = (P_{R0}, P_{\theta 0})$ will be at:

$$P_{\mathrm{R}}(t) = P_{\mathrm{R0}} + t\,V_{\mathrm{TR}} + t\,V_{\mathrm{EX}}\frac{r_{\mathrm{FR}}}{r_0}\cos(\phi-\theta),$$
$$P_{\theta}(t) = P_{\theta 0}. \tag{1}$$

Thus for $t > 0$, the flux rope magnetic field is in a non-force-free configuration. It is, however, assumed that for a given value of r_{FR}, the ratio of axial to poloidal magnetic field strengths is the same as in a force-free flux rope, with only the cross-sectional shape of the constant-α force-free flux rope modified. The magnetic field vector at a point (R, θ, Z) at a time t is then given by:

$$\begin{aligned}
\mathbf{B}(\hat{\mathbf{R}},\hat{\theta},\hat{\mathbf{Z}}) &= H\,B_0 J_1(\alpha r_{\mathrm{FR}})\frac{\partial\hat{\mathbf{P}}\partial\phi}{+}B_0 J_0(\alpha r_{\mathrm{FR}})\hat{\mathbf{Z}},\\
&= \left(H\,B_0 J_1(\alpha r_{\mathrm{FR}})\frac{\partial}{\partial\phi}\big[P_{\mathrm{R}}(t)\big]\right)\hat{\mathbf{R}} + \left(H\,B_0 J_1(\alpha r_{\mathrm{FR}})\frac{\partial}{\partial\phi}\big[P_{\theta}(t)\big]\right)\hat{\theta},\\
&\quad + B_0 J_0(\alpha r_{\mathrm{FR}})\hat{\mathbf{Z}}\\
&= H\,B_0 J_0(\alpha r_{\mathrm{FR}})\left(\frac{\partial P_{\mathrm{R0}}}{\partial\phi} + t\,V_{\mathrm{EX}}\frac{r_{\mathrm{FR}}}{r_0}\frac{\partial}{\partial\phi}\big[\cos(\phi-\theta)\big]\right)\hat{\mathbf{R}}\\
&\quad + H\,B_0 J_1(\alpha r_{\mathrm{FR}})\left(\frac{\partial P_{\theta 0}}{\partial\phi}\right)\hat{\theta} + B_0 J_0(\alpha r_{\mathrm{FR}})\hat{\mathbf{Z}}.
\end{aligned} \tag{2}$$

In this study it is assumed that V_{TR} is constant over the width of the flux rope. This is equivalent to assuming that the solar wind speed is constant over the flux rope extent, or that the flux rope cross section is largely unaffected by solar wind speed variations. Thus the model is most appropriate for events away from the fast/slow solar wind boundary or for events with a high internal pressure. The assumption of constant V_{TR} can be relaxed, but this does not lead to a significant improvement in flux rope fits to data, even for streamer belt events occurring at solar minimum (Owens, 2006).

The top panels of Figure 2 show the magnetic field components within a cross section of the model magnetic flux rope at four successive times (from left to right) during its evolution. Note that the value of the axial magnetic field, B_0, does not evolve with heliocentric distance, thus only the qualitative evolution of the magnetic field components should be considered. Black lines show contours of constant r_{FR} ($r_{\mathrm{FR}} = 1/3,\ 2/3$, and 1, respectively). On the far left of each panel, the initial force-free flux rope is of radius 1 R_{S} and is located 2 R_{S} above the photosphere. By the time the flux rope reaches 10 R_{S}, the kinematic propagation distorts the flux rope cross section into an elongated structure, while expansion increases the radial width of the flux rope cross section. The gradient in the magnetic field components, particularly B_θ, can be seen to increase as a result of this kinematic distortion, suggesting an increase in the current density. This is investigated further in Section 5. First we compare this magnetic field model with the magnetic cloud observations, including the event described in Section 2.

4. Comparison with Observations

Figure 3 shows the best model fits (red) to two magnetic clouds observed by the ACE spacecraft (black) during March 2001 (left) and November 2001 (right). See Owens, Merkin, and Riley (2006) and Owens (2006) for a description of the model fitting technique. Table 1 lists

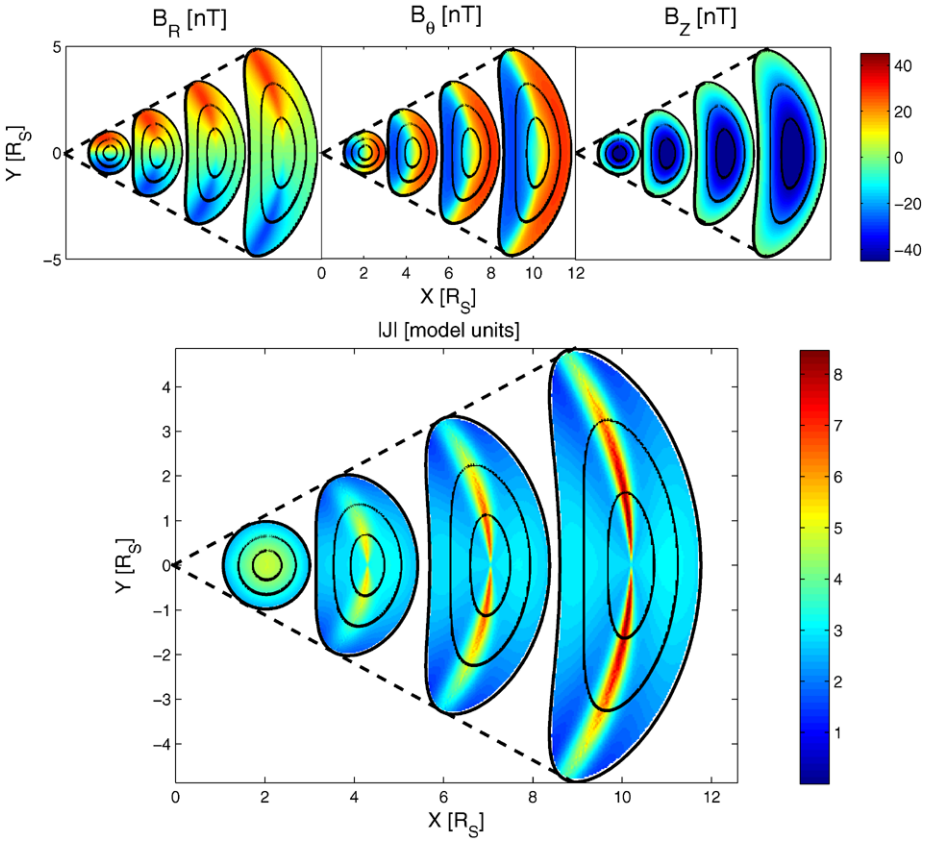

Figure 2 Top panels show the magnetic field components within a cross section of the model magnetic flux rope at four successive times (from left to right). The bottom panel shows the corresponding current density. Black lines show contours of constant r_{FR}. On the far left of each panel, the initial force-free flux rope is of radius 1 R_S and is located 2 R_S above the photosphere. By the time the flux rope reaches 10 R_S, the cross section has been flattened significantly and the magnetic field components are altered accordingly. Initially currents are volumetric, but by the time the flux rope reaches 10 R_S the current density is more sheet-like. This current sheet formation is purely the result of kinematic distortion.

the best-fit model parameters. There is good agreement between model and observed magnetic field time series for both events. In particular, the sharp discontinuities in the magnetic field components and angles observed near the centre of the magnetic clouds, indicative of thin current sheets, are well-reproduced by the model.

Figure 4 shows the model fits to the October 1998 and October 2003 magnetic clouds in the same format as Figure 3. The observed |**B**| profiles are highly asymmetric about the MC centres, which is likely to be the result of compression at the leading edge, an effect not incorporated in the analytical model. Consequently, the **B**-components are underestimated in the leading portions of the magnetic clouds. The direction of the magnetic field, as shown by the field angles, however, remain well-reproduced by the model. Furthermore, the sharp discontinuities close to the centre of the flux rope signatures are again matched by the model.

In all four magnetic clouds shown here, the large magnetic field discontinuity is consistent with kinematic distortion of the flux rope magnetic field. In order to statistically establish how often this signature is present in magnetic cloud observations it is useful to

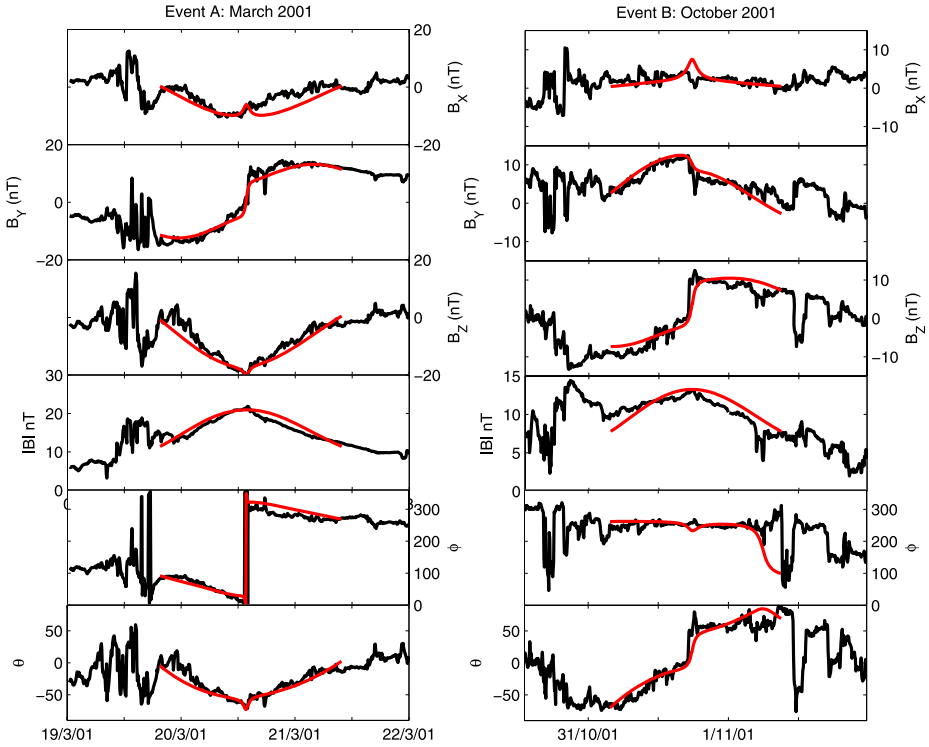

Figure 3 The best model fits (red) to two magnetic cloud observations (black) made by the ACE spacecraft during March 2001 (left) and November 2001 (right). The top three panels show the magnetic field components in GSE coordinates, followed by the magnetic field intensity. The bottom two panels show the angles of the magnetic field vector. There is good agreement between model and observed magnetic field time series, particularly the magnetic field discontinuities near the centre of the events.

define a parameter $\Delta\mathbf{B}$, the angular change in the magnetic field vector. Figure 5 shows a superposed epoch analysis of $\Delta\mathbf{B}$ using 30-min magnetic field data through all 197 magnetic clouds and cloud-like ICMEs listed in the updated Cane and Richardson (2003) catalogue. This analysis is sensitive to the precise identification of magnetic cloud boundaries, the flux rope orientation, and as will be shown in Section 5, the ICME angular extent and expansion. It will also be influenced by the erosion of magnetic flux from the magnetic cloud boundaries by magnetic reconnection, and the centre of the flux rope to better survive propagation to 1 AU. Despite the mitigating factors, there is some evidence for an increase in $\Delta\mathbf{B}$ close to the centre of magnetic clouds, suggesting the signature is not uncommon. The increase in $\Delta\mathbf{B}$ toward the front of magnetic clouds is likely the result of including some sheath and ICME leading edge features in the analysis. In Section 5, the model is used to compute the currents associated with these magnetic field configurations.

5. Currents in Magnetic Clouds

The electric current, $\mathbf{J}$, associated with a magnetic field configuration can be computed by taking the curl of $\mathbf{B}$. While it is not possible to compute such spatial derivatives from single-point spacecraft observations without further assumptions, we can readily compute $\mathbf{J}$ from

Table 1 The best-fit model parameters to the four magnetic cloud observations.

	W[a]	V_{EX}[b]	B_{AX}[c]	H[d]	ϕ_{AXIS}[e]	θ_{AXIS}[f]	Y[g]
Event A (March 2001)	61°	30 km s^{-1}	22 nT	−1	5°	−55°	−0.25
Event B (November 2001)	59°	25 km s^{-1}	15 nT	−1	85°	20°	−0.4
Event C (October 1998)	55°	25 km s^{-1}	20 nT	−1	140°	−25°	0.5
Event D (October 2003)	65°	75 km s^{-1}	42 nT	−1	340°	−50°	0.5

[a]The angular width of the flux rope.

[b]The expansion speed.

[c]The axial magnetic field strength.

[d]The magnetic helicity.

[e]The in-ecliptic angle of the axis to the X_{GSE} direction.

[f]The out-of-ecliptic angle of the axis to the Z_{GSE} direction.

[g]The closest approach of the spacecraft to the axis.

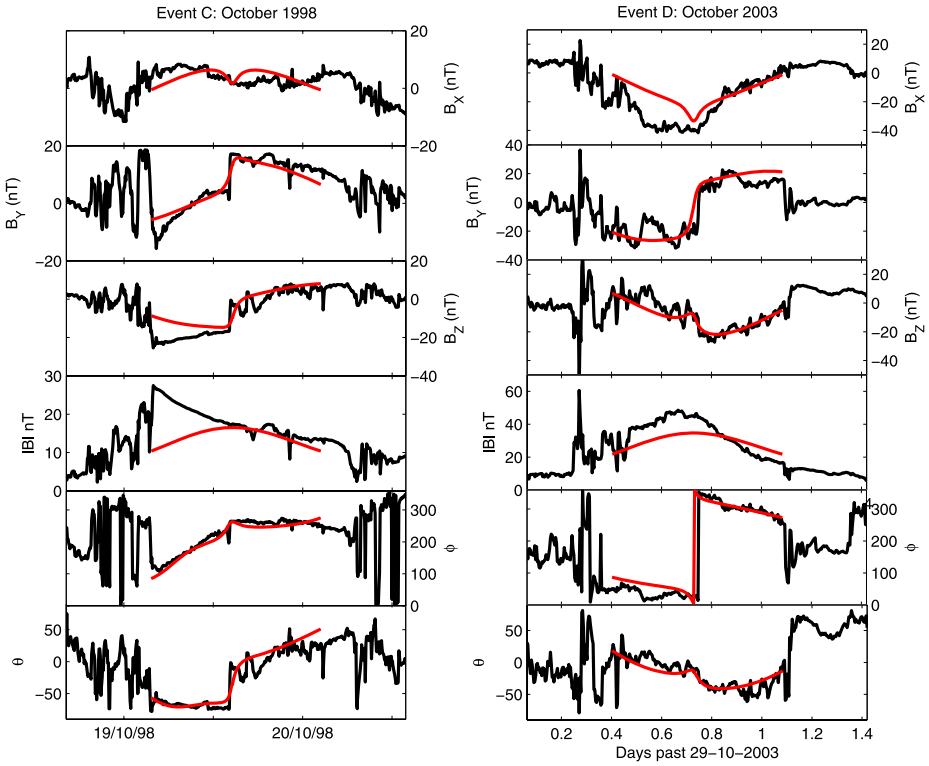

Figure 4 The best model fits (red) to two magnetic clouds observed by the ACE spacecraft (black) during October 1998 (left) and October 2003 (right), in the same format as Figure 3. Due to the asymmetric |**B**| profiles, the **B**-components are underestimated in the leading portions of the magnetic clouds. The direction of the magnetic field, as shown by the field angles, however, remains well-matched by the model.

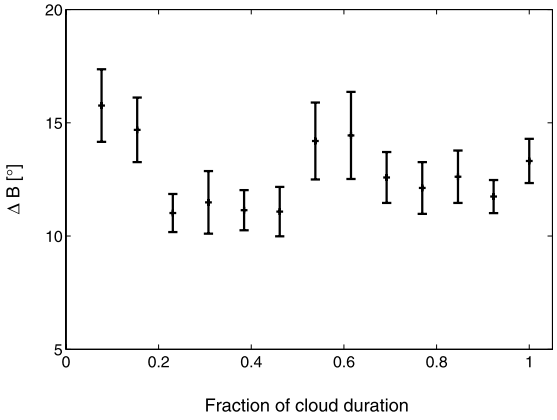

Figure 5 A superposed epoch analysis of the angular change in the magnetic field vector, $\Delta\mathbf{B}$, for 197 magnetic cloud and cloud-like ICMEs. This analysis is sensitive to the identification of magnetic cloud boundaries, the flux rope orientation, and as will be shown in Section 5, the ICME angular extent and expansion. Despite these mitigating factors, there is still some evidence for an increase in $\Delta\mathbf{B}$ close to the centre of magnetic clouds, suggesting such current sheets are not uncommon.

the model magnetic field. The bottom panel of Figure 2 shows the current density, $|\mathbf{J}|$, within a model magnetic flux rope at four different times during its near-Sun evolution. Note that the current density is shown in model units. As the axial magnetic field strength is set to match 1-AU observations and does not evolve with distance, however, the evolution of the current with heliocentric distance should only be considered in a qualitative sense. Black lines show contours of constant r_{FR}. On the far left, the initial force-free flux rope is of radius 1 R_{S} and is located 2 R_{S} above the photosphere. At this time currents are volumetric. By the time the flux rope reaches 10 R_{S}, however, the current is far more sheet-like. This current sheet formation results purely from the kinematic distortion of the flux rope.

The thickness and intensity of the current sheet at 1 AU depends on the extent to which the flux rope is distorted from its initial force-free state. Figure 6 shows the effect of varying expansion speed and CME angular width on the current density in the flux rope at 1 AU. The transit speed is 400 km s^{-1} in all cases. An angular width of 60° is used for the expansion speed variation, and an expansion speed of 50 km s^{-1} is used for the CME width variation. It can clearly be seen that current sheets are most intense for small expansion speeds and large CME angular widths, as these conditions maximise the distortion of the flux rope from its initial force-free state.

6. Discussion

In this study we demonstrate that large-scale current sheets observed close to the centre of magnetic clouds can arise due to purely kinematic effects, without the need for any external forcing. Four examples of such MC-associated current sheets, observed by the ACE spacecraft, were fit with an analytical model of a kinematically distorted magnetic flux rope. This simple model is found to reproduce the large-scale magnetic structure remarkably well, in particular the magnetic field discontinuities at the centres of the magnetic clouds. Numerical magnetohydrodynamic simulations of erupting flux ropes (*e.g.*, Riley *et al.*, 2004) may prove useful for further investigation of this effect. Additionally, Cluster observations of discontinuities within magnetic clouds (*e.g.*, Foullon *et al.*, 2007) may enable the currents to be directly computed and compared with the model predictions.

Using the magnetic flux rope model, current sheets are found to increase in intensity and gradient as the angular width of the flux rope increases and the expansion speed decreases.

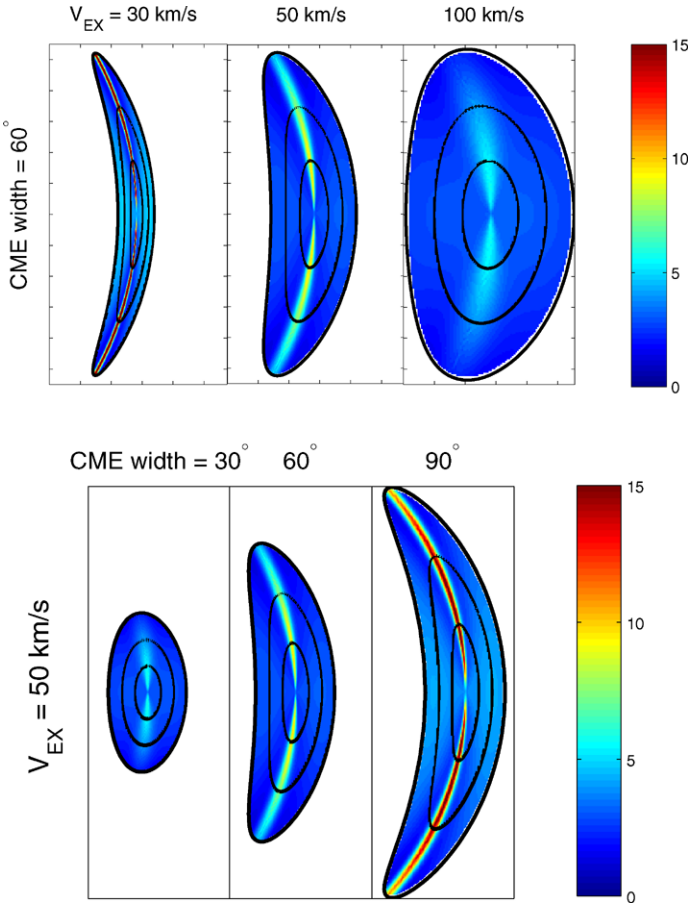

Figure 6 Current density, $|\mathbf{J}|$, within model magnetic flux ropes at 1 AU for different expansion speeds (top panels) and CME angular width (bottom panels). Current sheets are most intense for small expansion speeds and large angular extents, as this results in greater distortion from the initial force-free flux rope morphology.

Thus any magnetic reconnection across such large-scale current sheets is expected to occur most readily in large, slowly expanding magnetic clouds. Insufficient observations of magnetic reconnection within ICMEs (Gosling *et al.*, 2007) have yet to be gathered to test whether reconnection occurs preferentially within such ejecta.

Figure 7 shows a sketch of the possible consequence of magnetic reconnection across a current sheet produced at the centre of a magnetic cloud. The blue lines show the location of most intense current sheets. X-line formation and reconnection across these current sheets results in the single flux rope being fragmented into multiple (in the sketch show, three) smaller flux ropes (there is some observational evidence for multiple current sheets with a single ejection, *e.g.*, Osherovich, Fainberg, and Stone (1999) and Hu *et al.* (2004)). These smaller flux ropes are all closer to the force-free condition than the pre-existing flux rope, but maintain the same magnetic helicity. The smaller ropes will also have a reduced variation in field-line length between a 1-AU observer and the Sun, which may go some way to explain the lack of a flux rope signature in suprathermal electron observations (Owens, Crooker, and Horbury, 2009), and will directly affect energetic particle propagation. Note also that by

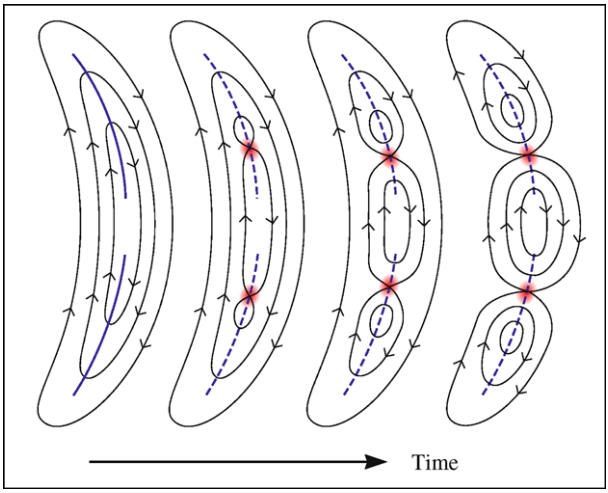

Figure 7 A sketch of the possible consequence of magnetic reconnection across a kinematically produced current sheet inside a magnetic cloud. The blue line shows the location of the most intense current sheet. X-line formation and reconnection across this current sheet results in the single flux rope being fragmented into multiple (in the sketch, three) smaller flux ropes.

fitting a single flux rope model to a multiple flux rope structure, the total flux content of a CME may be significantly underestimated, which has consequences for the role of CMEs in the evolution of the heliospheric magnetic field (Owens and Crooker, 2006). Well-separated multi-spacecraft observations of magnetic clouds, such as those provided by the STEREO mission, need to be analysed for evidence of multiple flux ropes within a single ejection.

Acknowledgements This research is funded by STFC (UK). I benefited from the availability of ACE magnetic field (PI: C. Smith) and SWEPAM (PI: D. McComas) data. I thank Tim Horbury and Robert Wicks of Imperial College London and Nancy Crooker of Boston University for useful discussions.

References

Burlaga, L.F.: 1988, *J. Geophys. Res.* **93**, 7217.
Burlaga, L.F., Sittler, E., Mariani, F., Schwenn, R.: 1981, *J. Geophys. Res.* **86**, 6673.
Cane, H.V., Richardson, I.G.: 2003, *J. Geophys. Res.* **108**(A4), SSH 6-1.
Collier, M.R., Szabo, A., Farrell, W.M., Slavin, J.A., Lepping, R.P., Fitzenreiter, R., *et al.*: 2001, *J. Geophys. Res.* **106**, 15985.
Crooker, N.U., Gosling, J.T., Smith, E.J., Russell, C.T.: 1990, In: Ressell, C.T., Priest, E.R., Lee, L.C. (eds.) *Physics of Magnetic Flux Ropes*, *AGU Geophys. Monogr.* **58**, 365.
Dere, K.P., Brueckner, G.E., Howard, R.A., Michels, D.J., Delaboudiniere, J.P.: 1999, *Astrophys. J.* **516**, 465.
Foullon, C., Owen, C.J., Dasso, S., Green, L.M., Dandouras, I., Elliott, H.A., Fazakerley, A.N., Bogdanova, Y.V., Crooker, N.U.: 2007, *Solar Phys.* **244**, 139.
Gopalswamy, N.: 2004, In: Poletto, G., Suess, S.T. (eds.) *The Sun and the Heliosphere as an Integrated System*, Kluwer Academic, Dordrecht, 201.
Gosling, J.T., Eriksson, S., McComas, D.J., Phan, T.D., Skoug, R.M.: 2007, *J. Geophys. Res.* **112**, A08106.
Hu, Q., Smith, C.W., Ness, N.F., Skoug, R.M.: 2004, *J. Geophys. Res.* **109**, A03102.
Hundhausen, A.J.: 1993, *J. Geophys. Res.* **98**, 13177.
Lepping, R.P., Jones, J.A., Burlaga, L.F.: 1990, *J. Geophys. Res.* **95**, 11957.
Low, B.C.: 1994, *Phys. Plasmas* **1**, 1684.
McComas, D.J., Gosling, J.T., Winterhalter, D., Smith, E.J.: 1988, *J. Geophys. Res.* **93**, 2519.
Newkirk, G. Jr., Hundhausen, A.J., Pizzo, V.: 1981, *J. Geophys. Res.* **86**, 5387.
Osherovich, V.A., Fainberg, J., Stone, R.G.: 1999, *Geophys. Res. Lett.* **26**, 401.
Owens, M.J.: 2006, *J. Geophys. Res.* **111**, A12109.
Owens, M.J.: 2008, *J. Geophys. Res.* **113**, A12102.
Owens, M.J., Crooker, N.U.: 2006, *J. Geophys. Res.* **111**, A10104.
Owens, M.J., Merkin, V.G., Riley, P.: 2006, *J. Geophys. Res.* **111**, A03104.

Owens, M.J., Crooker, N.U., Horbury, T.S.: 2009, *Ann. Geophys.*, in press.
Rees, A., Forsyth, R.J.: 2004, *Geophys. Res. Lett.* **31**, 6804.
Riley, P., Crooker, N.U.: 2004, *Astrophys. J.* **600**, 1035.
Riley, P., Linker, J.A., Lionello, R., Mikic, Z., Odstrcil, D., Hidalgo, M.A., Hu, Q., Lepping, R.P., Lynch, B.J., Rees, A.: 2004, *J. Atmos. Solar Terr. Phys.* **66**, 1321.
Russell, C.T., Jian, L.K., Luhmann, J.G.: 2009, *Geophys. Res. Lett.* **36**, L7105.
Rust, D.M.: 1994, *Geophys. Res. Lett.* **21**, 241.
Savani, N., Rouillard, A.P., Forsyth, R.J., Owens, M.J., Davies, J.A.: 2009, *Ann. Geophys.* submitted.
Schwenn, R., Dal Lago, A., Huttunen, E., Gonzalez, W.D.: 2005, *Ann. Geophys.* **23**, 1033.
St. Cyr., O.C., Howard, R.A., Sheeley, N.R. Jr., Plunkett, S.P., Michels, D.J., Paswaters, S.E., *et al.*: 2000, *J. Geophys. Res.* **105**, 18169.
Steed, K., Owen, C.J., Harra, L.K., Green, L.M., Dasso, S., Walsh, A.P., Démoulin, P., van Driel-Gesztelyi, L.: 2008, *AGU Fall Meeting*, Abstract No. 1638.